Journal of The
Electrochemical Society

Modelling the Through-Hole Coin Cell Configuration for *Operando* Optical Spectroscopy of Battery Electrodes

To cite this article: Oliver Rodríguez *et al* 2025 *J. Electrochem. Soc.* **172** 100517

Journal of The Electrochemical Society, 2025 **172** 100517

Modelling the Through-Hole Coin Cell Configuration for *Operando* Optical Spectroscopy of Battery Electrodes

Oliver Rodríguez, Rudra N. Samajdar, and Andrew J. Wain[*,z]

National Physical Laboratory, Teddington, Middlesex TW11 0LW, United Kingdom

Operando optical methods are widely used for measuring the properties of battery electrodes under charge/discharge conditions and provide valuable insights into various phenomena. However, the need to gain optical access to the electrode of interest often requires a compromise, such that the electrochemical characteristics of the operando cell deviate from those in a conventional cell. One approach towards minimally invasive optical spectroscopy is the "through-hole" coin cell configuration in which the bottom electrode is optically accessed via a hole punched through the top electrode and separator, but the impact of this hole on the validity of the measurement has been given little consideration. Here we performed modelling of graphite and lithium nickel manganese cobalt oxide ($LiNi_{0.6}Mn_{0.2}Co_{0.2}O_2$; NMC622) electrodes in a Li-ion half-cell arrangement, to explore this through-hole configuration. We show that the presence of a 0.5 mm radius hole results in a non-uniform Li^+ ion distribution in the electrode phase, but this can be reduced by decreasing the current, decreasing the hole size or increasing the separator thickness. The Li^+ non-uniformity varies non-linearly with the average degree of electrode lithiation and is more extreme for a graphite electrode compared to NMC622 due to their contrasting voltage-charge profiles.

 [DOI: 10.1149/1945-7111/ae0f54]

Manuscript submitted June 13, 2025; revised manuscript received September 10, 2025. Published October 13, 2025.

Supplementary material for this article is available online

Central to the development of improved electrochemical energy storage technologies is reliable materials characterisation. In particular, our ability to design and optimise new battery materials with improved capacity and lifetime requires an intimate grasp of their physical, structural and chemical properties, the measurement of which depends on advanced analytical science. *Operando* spectroscopy has a critical role to play in this context, enabling characterisation in real time during charge/discharge and thus yielding insights into a range of important phenomena including solid-electrolyte interphase (SEI) formation, ion intercalation, conversion reactions, redox processes, degradation pathways and failure mechanisms. From this perspective, optical techniques such as Raman spectroscopy have found particularly widespread application, which allow characterisation based on the electronic and/or vibrational properties of the material under investigation.

One of the many practical challenges in performing *operando* optical spectroscopy of electrochemical energy storage materials is the need to gain spectroscopic access to the internal components of the cell while minimising the impact on its electrochemical properties. Optical spectroscopy typically requires the introduction of a window that is transparent over the relevant wavelength range, and appropriate arrangement of the internal cell components so that there is an optical pathway to the electrode surface of interest with minimal losses via light absorption or scattering. These modifications can disrupt the potential distribution and flow of current within the cell, so there is often a compromise between the quality of the spectroscopic data generated and how well the electrochemical environment reflects that of a normal cell. Hence, optimising cell design and the internal cell configuration are important considerations for meaningful *operando* analysis.

Various different approaches to *operando* optical spectroscopy of battery materials have been reported.[1,2] A common method is to use a mesh or holed current collector, so that the active electrode material can be accessed optically from the rear side.[3–12] This method requires fabrication of a freestanding electrode or deposition of an electrode slurry directly onto bespoke current collectors, so is most suited to early-stage, small scale mechanistic studies. However, application of this approach to studying commercially-manufactured electrodes is limited, since these are typically supplied as pre-fabricated foil-backed electrode sheets. The distinction between lab-scale powders and commercially produced electrode sheets is important because the properties of composite electrodes are highly sensitive to the various processing steps involved in their manufacture (e.g., thermal cycling, calendering), such that the measured behaviour in these two scenarios almost always differs.

One method of performing *operando* optical spectroscopy on foil-backed electrodes is to cut a thin strip of the sample and place the active material face up against the spectroscopic window.[13–15] However, we reported in our previous experimental and modelling work that this arrangement results in significant disruption to current flow compared to a typical coin cell. This is due to blocked ion transport to the active face of the electrode under investigation, such that currents above ~C/30 cannot be reliably used without considerable loss in specific capacity.[16] Whilst we demonstrated that some of these limitations can be alleviated by simple introduction of a porous, holed spacer between the active material and the window, this configuration still differs considerably from the conventional battery arrangement in which the active sides of the positive and negative electrodes directly face each other.

An *operando* cell configuration that provides a solution to this problem is to arrange the electrodes in the conventional face-to-face orientation, but to punch a hole through one electrode and separator so the front face of the opposing electrode can be optically accessed (Fig. 1). This "through-hole" configuration, has been adopted successfully by several researchers and is among the more promising approaches to studying commercially-processed electrodes under realistic conditions using optical methods.[17–23] However, to date there has been little consideration of how the presence of the hole in the opposing electrode impacts the electrochemical properties of the cell and the local ion transport and intercalation/insertion processes taking place in the region being spectroscopically probed.

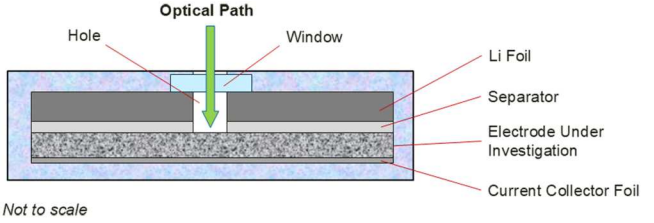

Figure 1. Schematic depiction of through-hole operando configuration for a Li-ion half-cell.

*Electrochemical Society Member.
zE-mail: andy.wain@npl.co.uk

In this work we use electrochemical modelling to explore the impact of the through-hole configuration on the potential, current and Li^+ ion distribution within a typical Li-ion half-cell with a standard 2032 coin cell form factor, with a view to better understanding the potential limitations of this technique and to guide selection of experimental parameters. We compare the behaviour of graphite and lithium nickel manganese cobalt oxide ($LiNi_{0.6}Mn_{0.2}Co_{0.2}O_2$; NMC622) as typical negative and positive electrode materials, respectively, and demonstrate that presence of the hole in the Li foil counter electrode leads to a non-uniform Li^+ distribution in the electrode under investigation, the extent of which depends on several experimental variables.

Modelling

The through-hole *operando* configuration was modelled in COMSOL Multiphysics 6.2 using the Lithium-Ion Battery Interface;[24] a simplified schematic of the geometry is shown in Fig. 2. Full details of the model are described in the Supplementary Information (SI) section S1 and Fig. S1. In brief, the interface solves the equations for the charge and mass balances in the electrodes and electrolyte, while current continuity between the working electrode and the electrolyte is ensured using the Butler-Volmer equation, with the exchange current density defined by a lithium insertion expression.

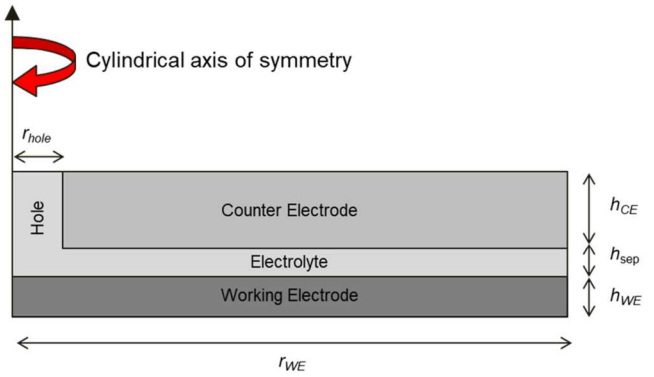

Figure 2. Schematic cross section depiction of through-hole model.

Table I shows the key parameters used in the simulations (a full list of parameters is presented in SI section S1). In practice the working electrode radius would be 7 mm, reflecting a typical 2032 coin cell form factor, but in order to decrease the computational demand and improve model convergence a reduced radius of 2.5 mm was used for the simulations (note this is a conservative scenario in which the area ratio of hole to electrode is larger than in the real case). Comparison of simulated data generated by the full scale and reduced size models showed that this reduction in size had no noticeable effect on the validity of the model (see Fig. S2a). Hole radii of 0.25 mm and 0.5 mm were explored as the minimum practically feasible hole sizes. Working electrode thicknesses were based on typical values for commercially produced graphite and NMC622 electrodes while ignoring the thickness of the foil current collector. Two separator thicknesses were simulated: one at 25 μm thick, representing a typical microporous separator used in standard coin cells, and one at 300 μm thick, representing a thicker glass fibre separator also used by some research groups in *operando* cells (we note that after wetting and under compression, a 300 μm thick glass fibre separator would likely decrease in thickness, but we use this value to represent the upper extreme case).

Table I. Key parameters used in model.

	Parameter	Value
r_{WE}	Cell radius	2.5 mm
r_{hole}	Hole radius	0, 0.25 mm or 0.50 mm
h_{WE}	Working electrode thickness	25 μm, 50 μm, 75 μm (graphite) or 42 μm (NMC)
h_{CE}	Counter electrode thickness	120 μm
h_{sep}	Separator thickness	25 μm or 300 μm

Results and Discussion

Electrochemical behaviour of through-hole configuration.— We begin by assessing the influence of introducing a hole into a graphite-Li half-cell on its electrochemical properties (Figs. S2b–S2d). Simulated cell voltage curves demonstrate that for a hole radius of 0.5 mm, for a given current the electrochemical response is not visibly changed compared to that in the absence of a hole (Fig. S2b). A change in current from 0.1 C to 1 C does result in a marginal decrease in graphite electrode utilisation, and this difference can be seen more clearly in the differential capacity/voltage profiles between these currents (Figs. S2c–S2d), but in all cases the presence of the hole has a negligible effect on the global cell electrochemical properties. Whilst this is fully expected given that a 0.5 mm radius hole only represents <0.5% of the total electrode area, we considered this an important control simulation to support the concept of the through-hole configuration as a minimally invasive approach.

Graphite electrode lithiation profiles in through-hole half-cell.— The model was next used to simulate the distribution of intercalated Li^+ through the full depth of a 50 μm thick graphite electrode in a half-cell arrangement during lithiation, in order to assess the impact of the hole in the opposing Li counter electrode on the extent of local electrode utilisation. Figure 3 depicts representative cross sections of the intercalated Li^+ distribution through the graphite electrode at 50% average degree of lithiation (equivalent to 50% stochiometric state of charge) during half-cell discharge under different conditions. In the cross sections shown, the top of the electrode is in contact with the separator, while the bottom of the electrode connects to the non-porous current collector. At 1 C (Figs. 3a–3c) a negative gradient in Li^+ concentration is observed through the depth of the electrode, reflecting Li^+ transport limitations through the porous electrode phase. The extent of Li^+ excess at the top appears to be similar for hole radii of 0.5 mm and 0.25 mm (compare Figs. 3a and 3b), but is slightly less pronounced for the thicker separator (Fig. 3c). No clear depth gradient is visible at 0.1 C (Fig. 3d) since the longer experimental timescale allows the Li^+ distribution to homogenise. More importantly, in all cases the radially central region of the electrode (corresponding to the left-hand side of the plots in Fig. 3) exhibits a significantly lower Li^+ concentration compared to the rest of the electrode, the extent of which depends on the geometric parameters used. Decreasing the hole radius from 0.5 mm (Fig. 3a) to 0.25 mm (Fig. 3b) results in a less extensive degree of "under-lithiation" both in terms of the lower limit of Li^+ concentration and how far the under-lithiated zone extends radially into the electrode away from the centre. Increasing the separator thickness from 25 μm to 300 μm (Fig. 3c) or reducing the current to 0.1 C (Fig. 3d) also have the effect of partially alleviating the extent of under-lithiation but there is still clear evidence of a lower Li^+ concentration in the radially central region. We also note that similar behaviour was observed with different thicknesses of graphite electrode (Fig. S3), with the through-depth Li^+ gradient becoming more pronounced with increased thickness, as expected.

The observed behaviour reflects a local ion transport hysteresis, owing to the absence of a counter electrode and source of Li^+ ions directly opposite the radially central region of the graphite electrode, thus resulting in a greater distance between the counter and working electrode in this central region (up to ~0.5 mm) compared to the remainder of the cell (25 μm or 300 μm). This results in a radial

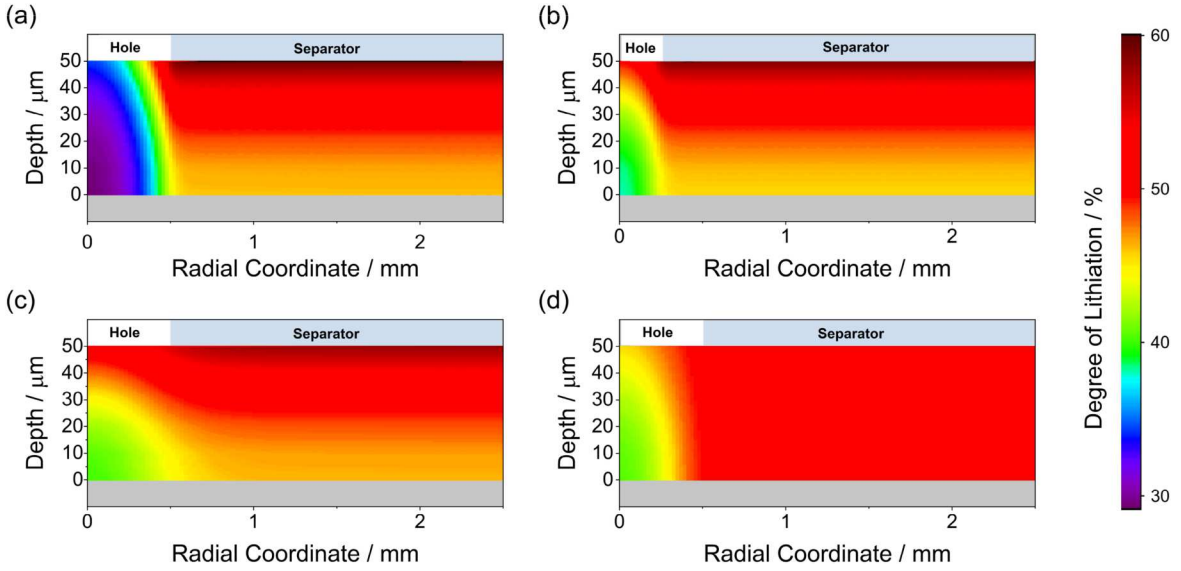

Figure 3. Simulated lithiation profiles through the depth of a graphite electrode (h_{WE} = 50 μm) in through-hole half-cell, showing local degree of lithiation at 50% average degree of lithiation during discharge. (a) r_{hole} = 0.5 mm, h_{sep} = 25 μm, current = 1 C; (b) r_{hole} = 0.25 mm, h_{sep} = 25 μm, current = 1 C; (c) r_{hole} = 0.5 mm, h_{sep} = 300 μm, current = 1 C; (d) r_{hole} = 0.5 mm, h_{sep} = 25 μm, current = 0.1 C.

potential gradient within the electrolyte phase filling the hole, which is of the order of 50 mV at an average degree of lithiation of 50% (Fig. S4a). Similarly, the presence of the hole introduces a non-uniformity in the current distribution, with the counter electrode delivering more local current from around the circumference of the hole by as much as a factor of two (Fig. S4b). Increasing the separator thickness from 25 μm to 300 μm provides a greater distance over which the Li^+ distribution can homogenise in the electrolyte phase, leading to a less extreme potential gradient and a decrease in the observed Li^+ depletion in the solid phase. This is somewhat counterintuitive because it suggests that increasing the cell resistance is favourable in terms of the resulting Li^+ distribution, but this will be at the cost of overall cell electrochemical performance. Use of a lower current significantly reduces the observed local hysteresis quite simply because it allows more time for Li^+ diffusion into the depleted region.

The depth profiles shown in Fig. 3 indicate that the observed under-lithiation is most extreme at the bottom of the electrode where it contacts the current collector, owing to the limited rate of Li^+ transport through the graphite. However, in an *operando* optical spectroscopy experiment adopting the through-hole configuration it would only be the top face of the electrode that is subject to spectroscopic analysis. Therefore, to assess the potential impact of the non-uniform lithiation on the *operando* spectroscopy, we determined the degree of lithiation at a depth of just 1 μm from the top of the electrode; whilst the penetration depth of optical techniques varies with material and excitation wavelength, this was considered to be a reasonable estimate of the measurement sampling depth that would be broadly applicable to most scenarios. Figure 4 shows the local degree of lithiation taken at a depth of 1 μm from the top of the graphite electrode over the full range of simulated average degrees of lithiation and two different currents. In all cases a decrease in the degree of lithiation is observed towards the radially central region of the electrode, consistent with the depth profiles in Fig. 3.

The most noteworthy observation from Fig. 4 is that the extent of non-uniformity in Li^+ distribution varies in an irregular fashion with average degree of lithiation. The extent of this irregularity is most pronounced at 0.1 C (Fig. 4b) where the most extreme relative decrease in degree of lithiation in the radially central region is observed at roughly 40% and 80% average degree of lithiation, while at 50% average degree of lithiation the lateral Li^+ distribution is relatively homogeneous. This behaviour can be seen more clearly in Fig. 4c, in which the degree of lithiation simulated at the radial centre of the graphite electrode is ratioed against that simulated at the radial edge of the electrode, and the relative minima at ~40% and ~80% average degree of lithiation are evident.

This behaviour can be understood by considering the balance between Li^+ transport and kinetic bottlenecks owing to phase transitions within the lithiated graphite. Like many Li^+ intercalation/insertion materials, lithiated graphite is a staging material in which phase separation occurs in a manner characterised by the Li:C stoichiometry. For example, when the degree of lithiation is above 50% an active equilibrium exists between fully lithiated LiC_6 phases and $Li_{0.5}C_6$ phases in which only alternate graphene layers are occupied by Li^+, while at lower intercalated lithium concentrations the LiC_6 phase no longer occurs and new, more dilute lithiated phases emerge. The detailed structure of the various phases of lithiated graphite will not be discussed here, but the key consideration is that transitions between active phase equilibria are associated with discrete changes in the graphite electrode potential and come with kinetic limitations.[25–28] Returning to Fig. 4c, the fact that the non-uniformity in Li^+ distribution resulting from the opposing hole appears to become less extreme at an average degree of lithiation of 50% compared to 40%, for example, can be rationalised by the occurrence of a marked transition between active phase equilibria at this point, during which the lithiation process is kinetically limited, rather than Li^+ transport controlled. This has the effect of reducing the lag in lithiation of the radially central region of the electrode and in simple terms allows the under-lithiated zone to equilibrate with the remainder of the electrode. The correlation between the degree of Li^+ non-uniformity and phase transitions can be seen by comparing the relative degree of lithiation with the simulated dV/dQ plot (Fig. 4d), wherein peaks in dV/dQ can be seen to coincide with minima in the relative difference in state of lithiation between the radial centre and the edge of the electrode. The observation that the variation in non-uniformity with average degree of lithiation is more pronounced at 0.1 C than 1 C can be explained by the fact that at 0.1 C there is more time for homogenisation in the Li distribution during the voltage-limited bottlenecks.

NMC electrode lithiation profiles in through-hole half-cell.—To explore how the above phenomenon is affected by the nature of the sample under study, equivalent simulations were performed for an NMC working electrode, representing a typical positive electrode material for Li-ion batteries. The results are shown in Fig. 5, which

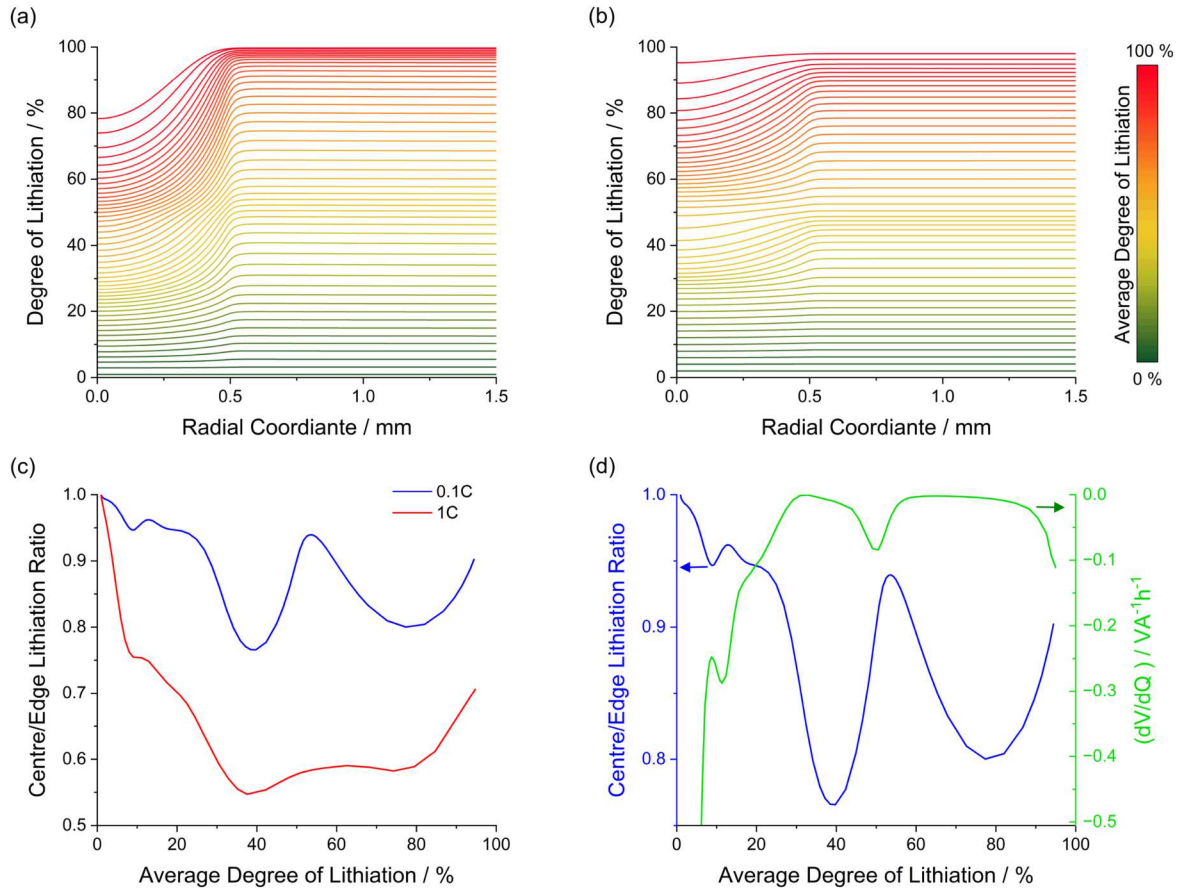

Figure 4. Simulated lithiation profiles at a depth of 1 μm from the top of a graphite electrode in a through-hole half-cell (r_{hole} = 0.5 mm, h_{sep} = 25 μm, h_{WE} = 50 μm) at different average degrees of lithiation and currents of (a) 1 C and (b) 0.1 C. (c) Ratio of simulated degree of lithiation at the radial centre of the electrode, to that simulated at the outermost radial edge at a depth of 1 μm, plotted as a function of average degree of lithiation. (d) 0.1 C data from part (c) plotted alongside dV/dQ for the same current.

are equivalent to the data presented in Fig. 4 but for the NMC material, depicting the degree of lithiation at a depth of 1 μm from the top of the electrode (Figs. 5a and 5b), the relative lithiation ratio from the centre to the edge of the electrode (Fig. 5c) and the same ratio plotted alongside the simulated dV/dQ curve for the NMC-Li cell (Fig. 5d).

The most notable observation upon comparing Figs. 5 to 4 is that the extent of under-lithiation observed at the radial centre of the electrode is considerably less pronounced for the NMC compared to the graphite electrode. This can be seen most clearly in Fig. 5c, in which the minimum lithiation ratio between the centre and the edge of the electrode at 1 C is approximately 0.85, whereas for graphite this is roughly 0.55. As with the graphite working electrode, the shape of the profiles in Fig. 5c can be understood by comparison against the dV/dQ plot (Figs. 5d and S5); in the case of NMC the phase transitions are manifested in notably more broad features in the dV/dQ plot compared to graphite, but there is nevertheless a correlation between these features and the extent of under-lithiation in the radial centre of the electrode.

To explore the underlying reasons for the less pronounced under-lithiation in the case of NMC compared to graphite, we performed simulations in which key materials properties were independently varied. Specifically, we focused on properties that were markedly different between NMC and graphite, and thus might provide a rationale for their differing behaviours. We found that the extent of the Li^+ non-uniformity was broadly insensitive to the Li^+ diffusion coefficient in the solid phase and the electrical conductivity of the active material (Figs. S6 and S7, respectively), suggesting that these were not individually responsible for the observed differences. We varied the Li^+ insertion kinetics (Fig. S8) and observed some changes in Li^+ non-uniformity in the case of graphite (Fig. S8a), but very little change in the case of NMC (Fig. S8b) across three orders of magnitude in exchange current density; whilst this contrasting behaviour is an interesting observation, the fact that the Li^+ non-uniformity remains low for all simulated exchange current densities for NMC suggests that insertion kinetics are not the primary governing factor. Bearing in mind the observed sensitivity to dV/dQ in Figs. 4d and 5d, we finally considered the differing voltage-charge behaviours of graphite and NMC as a source of the contrasting responses in terms of Li^+ non-uniformity. While graphite is characterised by a largely very shallow voltage-charge profile after an initial, sharp voltage drop (Fig. S2a), NMC exhibits a more gradual decrease in voltage with degree of lithiation (Fig. S5a). This can be seen more quantitatively from the dV/dQ behaviour; for graphite at 0.1 C, the magnitude of dV/dQ is less than 0.1 V A^{-1} h^{-1} for the majority of the lithiation profile and falls below 0.01 V A^{-1} h^{-1} in the plateau regions (Fig. S2d), while for NMC, the magnitude of dV/dQ is notably higher (between 0.1 V A^{-1} h^{-1} and 0.5 V A^{-1} h^{-1}). The result of this is that graphite lithiation is not voltage-limited across a wide range of states of charge, so we propose that under these conditions the depleted availability of Li^+ resulting from the hole in the Li counter electrode has a significant impact on Li^+ uniformity in the graphite electrode (hence the Li^+ non-uniformity being most pronounced in the plateau regions of the voltage-charge profile). On the other hand, the lithiation of NMC is more voltage-limited across all states of charge which prevents the unavailability of Li^+ in the region opposite the hole from significantly impacting the distribution of Li^+ in the solid electrode phase. To confirm the governing role of the voltage-charge behaviour on the Li^+ non-uniformity, we performed simulations using different hypothetical voltage-charge profiles, two in which the voltage drop is

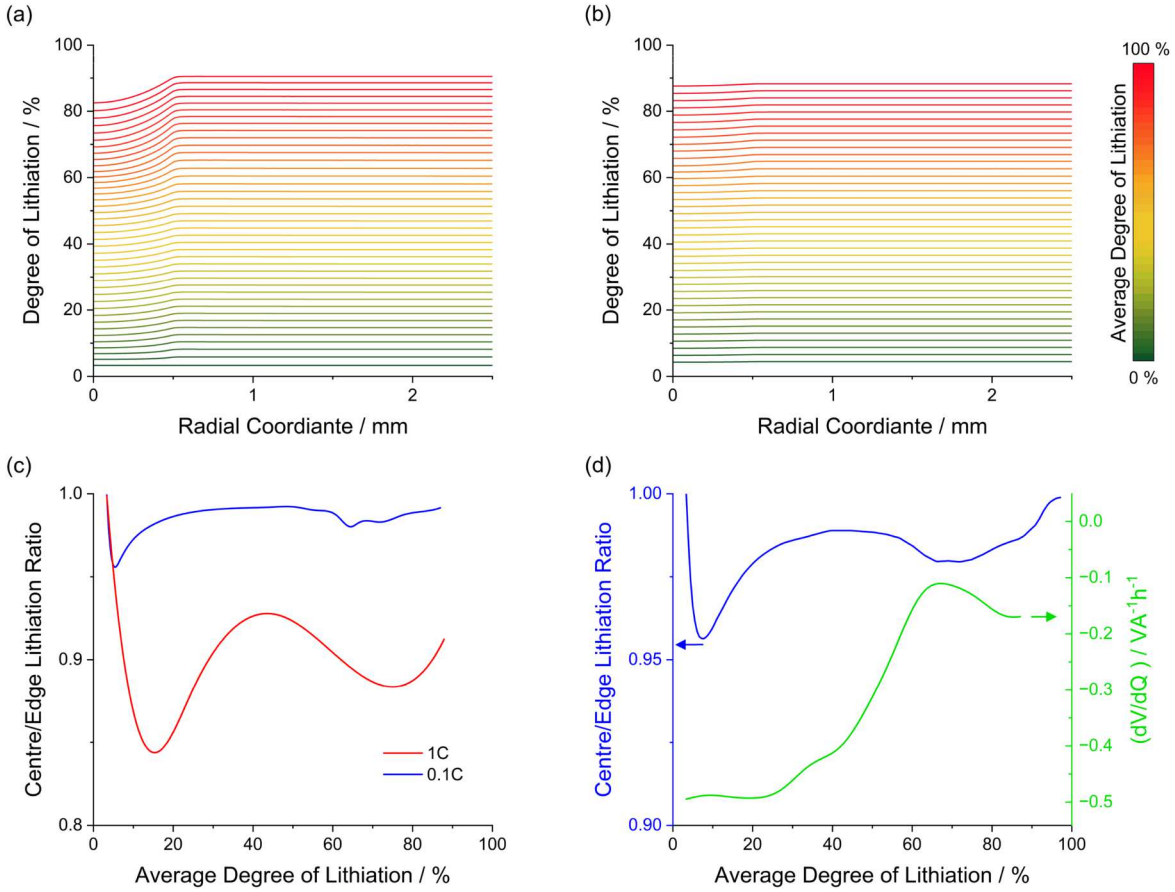

Figure 5. Simulated lithiation profiles at a depth of 1 μm from the top of an NMC622 electrode in a through-hole half-cell ($r_{hole} = 0.5$ mm, $h_{sep} = 25$ μm, $h_{WE} = 42$ μm) at different average degrees of lithiation and currents of (a) 1 C and (b) 0.1 C. (c) Ratio of simulated degree of lithiation at the radial centre of the electrode, to that simulated at the outermost radial edge at a depth of 1 μm, plotted as a function of average degree of lithiation. (d) 0.1 C data from part (c) plotted alongside dV/dQ for the same current.

very shallow across most states of charge, and one with a constant voltage-charge gradient, keeping all other parameters constant. As shown in Fig. S9, in the case of the mostly shallow voltage profiles the Li^+ non-uniformity is much more pronounced than in the case of the constant voltage-charge gradient, supporting our hypothesis that the voltage-charge behaviour is a dominant factor.

Conclusions

We have demonstrated through simulation that particular care needs to be taken when performing *operando* spectroscopy of battery materials using the through-hole optical approach. While the global electrochemistry of a half-cell with 2032 form factor is largely unaffected by the presence of a 0.5 mm radius hole in the Li electrode, the absence of a counter electrode opposite the working electrode does result in a non-uniform Li^+ concentration in the solid phase, such that the zone under spectroscopic analysis is under-lithiated compared to the surrounding electrode. The extent of this non-uniformity varies in a complex way with the total degree of lithiation (and hence state of charge) owing to the staging or phase transition behaviour of the electrode material. The predicted non-uniformity is most prominent at high currents, so low current (e.g., <0.1 C) cycling conditions are recommended for use with this configuration. The effects of the observed phenomenon can also be alleviated by minimizing the size of the hole (although this may be practically very challenging) or increasing the thickness of the separator (which may be experimentally easy to implement but would be expected to eventually have a deleterious effect on cell performance due to increased resistance). The extent of the non-uniformity in lithiation is highly sensitive to the electrochemical properties of the electrode material, with graphite exhibiting more pronounced under-lithiation at the centre compared to NMC, resulting from the more voltage-limited behaviour of the latter. This is an important observation because it suggests that more care needs to be taken when using the through-hole optical approach to study ideal intercalation/insertion materials which have pronounced voltage-charge plateaus.

This work highlights the importance of carefully considering the internal conditions of the cell when performing measurements in bespoke *operando* cells that deviate from a standard geometry. Even a small modification of the cell for the purpose of gaining optical access can potentially have a significant impact on the localised behaviour and potentially undermine spectral interpretation. For the through-hole configuration, the extent of lithiation and electrode potential differ locally at the centre compared to the average state of charge and global cell potential, and this deviation is most significant at the position that is being probed spectroscopically. As a result, it is possible that false correlations between state of charge or cell voltage and changes in the spectroscopic response are made. This also potentially affects the use of *operando* optical cells in this configuration for long term ageing studies, since the central region of the electrode will be subject to a less extreme load (in terms of potential or extent of lithiation) than the remainder of the cell, potentially generating misleading inferences. We note that our work only considers the influence of the hole on the response and does not account for the impact of introducing a window into the cell body, which has been shown experimentally to affect the localised chemical changes occurring.[29] Furthermore, our model does not explicitly consider the effect of local heterogeneities inherent to the electrode under study, for example due to its composite nature or

spatial variations resulting from the manufacturing process, which may be significant contributors to non-uniform Li^+ distribution during experimental studies.

The work presented herein serves as a demonstration of the value of using modelling to guide and optimise experimental design, allowing these potentially problematic effects to be minimised. While this work has been purely based on simulation, we do have experimental evidence demonstrating practical manifestation of the predicted non-uniformity, and this will be the topic of a separate publication.

Acknowledgments

This work was supported by the project 21GRD01 (OpMetBat), which received funding from the European Partnership on Metrology, cofinanced by the European Union's Horizon Europe Research and Innovation Programme and by the Participating States. The authors also acknowledge support from the National Measurement System of the UK Department of Science, Innovation and Technology. The authors are indebted to Edmund Dickinson, About Energy Ltd, for his early contribution to this work and helpful discussions since. We also thank Pierre Kubiak (NPL) for his constructive feedback on the manuscript.

ORCID

Oliver Rodríguez https://orcid.org/0000-0003-2350-1214
Rudra N. Samajdar https://orcid.org/0000-0002-5737-4906
Andrew J. Wain https://orcid.org/0000-0002-8666-6158

References

1. L. Meyer, N. Saqib, and J. Porter, "Review-operando optical spectroscopy studies of batteries." *J. Electrochem. Soc.*, **168**, 090561 (2021).
2. P. Novák, J. C. Panitz, F. Joho, M. Lanz, R. Imhof, and M. Coluccia, "Advanced in situ methods for the characterization of practical electrodes in lithium-ion batteries." *J. Power Sources*, **90**, 52 (2000).
3. D. C. Chen, M. A. Mahmoud, J. H. Wang, G. H. Waller, B. T. Zhao, C. Qu, M. A. El-Sayed, and M. L. Liu, "Operando investigation into dynamic evolution of cathode-electrolyte interfaces in a Li-Ion battery." *Nano Lett.*, **19**, 2037 (2019).
4. N. E. Drewett, I. M. Aldous, J. L. Zou, and L. J. Hardwick, "In situ Raman spectroscopic analysis of the lithiation and sodiation of antimony microparticles." *Electrochim. Acta*, **247**, 296 (2017).
5. E. Flores, P. Novák, and E. J. Berg, "In situ and *Operando* Raman spectroscopy of layered transition metal oxides for Li-ion battery cathodes." *Frontiers in Energy Research*, **6**, 82 (2018).
6. L. J. Hardwick, H. Buqa, and P. Novák, "Graphite surface disorder detection using in situ Raman microscopy." *Solid State Ionics*, **177**, 2801 (2006).
7. T. Kim, L. K. Ono, and Y. B. Qi, "Understanding the nucleation and growth of the degenerated surface structure of the layered transition metal oxide cathodes for lithium-ion batteries by operando Raman spectroscopy." *J. Electroanal. Chem.*, **915**, 116340 (2022).
8. N. Mozhzhukhina, E. Flores, R. Lundström, V. Nyström, P. G. Kitz, K. Edström, and E. J. Berg, "Direct *Operando* observation of double layer charging and early solid electrolyte interphase formation in Li-ion battery electrolytes." *J. Phys. Chem. Lett.*, **11**, 4119 (2020).
9. A. R. Neale, D. C. Milan, F. Braga, I. V. Sazanovich, and L. J. Hardwick, "Lithium insertion into graphitic carbon observed via operando Kerr-Gated Raman spectroscopy enables high state of charge diagnostics." *ACS Energy Lett.*, **7**, 2611 (2022).
10. P. Novák, D. Goers, L. Hardwick, M. Holzapfel, W. Scheifele, J. Ufhiel, and A. Würsig, "Advanced in situ characterization methods applied to carbonaceous materials." *J. Power Sources*, **146**, 15 (2005).
11. C. Sole, N. E. Drewett, and L. J. Hardwick, "In situ Raman study of lithium-ion intercalation into microcrystalline graphite." *Faraday Discuss.*, **172**, 223 (2014).
12. H. M. Xie, H. B. Song, J. G. Guo, Y. L. Kang, W. Yang, and Q. Zhang, "In situ measurement of rate-dependent strain/stress evolution and mechanism exploration in graphene electrodes during electrochemical process." *Carbon*, **144**, 342 (2019).
13. S. J. Harris, A. Timmons, D. R. Baker, and C. Monroe, "Direct in situ measurements of Li transport in Li-ion battery negative electrodes." *Chem. Phys. Lett.*, **485**, 265 (2010).
14. J. L. Lei, F. McLarnon, and R. Kostecki, "In situ Raman microscopy of individual $LiNi_{0.8}Co0_{.15}Al_{0.05}O_2$ particles in a Li-ion battery composite cathode." *J. Phys. Chem. B*, **109**, 952 (2005).
15. Visualizing the potential gradient in a graphite electrode during electrochemical lithiationEL-CELL, (2017), https://el-cell.com/visualizing-the-potential-gradient-in-a-graphite-electrode-during-electrochemical-lithiation/.
16. T. E. Rosser, E. J. F. Dickinson, R. Raccichini, K. Hunter, A. D. Searle, C. M. Kavanagh, P. J. Curran, G. Hinds, J. Park, and A. J. Wain, "Improved operando Raman cell configuration for commercially-sourced electrodes in Alkali-Ion batteries." *J. Electrochem. Soc.*, **168**, 070541 (2021).
17. F. S. Gittleson, K. P. C. Yao, D. G. Kwabi, S. Y. Sayed, W. H. Ryu, Y. Shao-Horn, and A. D. Taylor, "Raman spectroscopy in lithium-oxygen battery systems." *Chemelectrochem*, **2**, 1446 (2015).
18. N. Gogoi, T. Melin, and E. J. Berg, "Elucidating the step-wise solid electrolyte interphase formation in lithium-ion batteries with operando raman spectroscopy." *Adv. Mater. Interfaces*, **9**, 2200945 (2022).
19. T. Gross, L. Giebeler, and C. Hess, "Novel in situ cell for Raman diagnostics of lithium-ion batteries." *Rev. Sci. Instrum.*, **84**, 073109 (2013).
20. S. Hy, Felix, Y.-H. Chen, J.-y Liu, J. Rick, and B.-J. Hwang, "In situ surface enhanced Raman spectroscopic studies of solid electrolyte interphase formation in lithium ion battery electrodes." *J. Power Sources*, **256**, 324 (2014).
21. P. Jehnichen and C. Korte, "Operando Raman spectroscopy measurements of a high-voltage cathode material for lithium-ion batteries." *Anal. Chem.*, **91**, 8054 (2019).
22. Y. Miroshnikov and D. Zitoun, "Operando plasmon-enhanced Raman spectroscopy in silicon anodes for Li-ion battery." *J. Nanopart. Res.*, **19**, 372 (2017).
23. J. S. Weaving, A. Lim, J. Millichamp, T. P. Neville, D. Ledwoch, E. Kendrick, P. F. McMillan, P. R. Shearing, C. A. Howard, and D. J. L. Brett, "Elucidating the sodiation mechanism in hard carbon by operando Raman spectroscopy." *ACS Appl. Energy Mater.*, **3**, 7474 (2020).
24. COMSOL AB, Stockholm, SwedenCOMSOL Multiphysics® v. 6.2, (2023), https://www.comsol.com.
25. J. R. Dahn, "Phase diagram of Li_xC_6." *Physical Review B*, **44**, 9170 (1991).
26. H. Fujimoto, T. Yamaki, K. Shimoda, S. Fujinami, T. Nakatani, G. Kano, M. Kawasaki, Z. Ogumi, and T. Abe, "Phase diagram of Li-Graphite intercalation compound formed by the charge/discharge reaction in Li-Ion battery." *J. Electrochem. Soc.*, **169**, 070507 (2022).
27. A. Funabiki, M. Inaba, T. Abe, and Z. Ogumi, "Stage transformation of lithium-graphite intercalation compounds caused by electrochemical lithium intercalation." *J. Electrochem. Soc.*, **146**, 2443 (1999).
28. A. M. Dimiev, K. Shukhina, N. Behabtu, M. Pasquali, and J. M. Tour, "Stage transitions in graphite intercalation compounds: role of the graphite structure." *The Journal of Physical Chemistry C*, **123**, 19246 (2019).
29. O. J. Borkiewicz, K. M. Wiaderek, P. J. Chupas, and K. W. Chapman, "Best practices for operando battery experiments: influences of X-ray experiment design on observed electrochemical reactivity." *The Journal of Physical Chemistry Letters*, **6**, 2081 (2015).